

*OK of General 10.6.10*

# Improving Ground Motion Attenuation Relation in the Great Basin

## Final Technical Report

Project: 06HQGR0006, *Colorado School of Mines*

Feng Su

US Bureau of Reclamation  
Denver Federal Center  
Denver, CO 80225  
Phone: (303) 445-3209  
Fax: (303) 445-6478  
E-mail: fsu@usbr.gov

Submitted to the  
U.S. GEOLOGICAL SURVEY

September, 2010

## Project Title: Improving Ground Motion Attenuation Relation in the Great Basin

(USGS Grant #: 06HQGR0006)

The objective of this project is to develop ground motion attenuation relations suitable for the Great Basin by constraining path effect using empirical and synthetic data from the Great Basin and by constraining source effect using source parameters derived from events of extensional environment. In general, our efforts have been focused on: (1) further validating and improving our numerical procedure for synthetic strong motion simulation, (2) understanding source effect on attenuation relations, and (3) study of local and regional seismic wave propagation for the Great Basin area in order to better simulate scenario ground motions useful for developing ground motion attenuation relations based on combined empirical and synthetic data from the Great Basin.

To further validate our numerical simulation procedures, we have carefully studied six relatively well-recorded  $M > 6.5$  earthquakes, namely the 1971 Imperial Valley earthquake, the 1989 Loma Prieta earthquake, the 1992 Landers earthquake, the 1994 Northridge earthquake, the 1995 Kobe earthquake, and the 1999 Kocaeli earthquake. We used the composite source simulation procedure (Zeng et al., 1994) to calculate the synthetic ground motions at all the collected stations. Figure 1 plots the misfit between the observation and synthetic prediction for the horizontal components for the Northridge earthquake. The misfit is quantified in terms of biases (upper panel) and standard errors (lower panel) over a broad frequency range. The middle line in the upper panel of Figure 1 shows the biases versus frequencies with the 90% confidence level envelopes of the biases. The comparison between synthetics and observations suggests that the composite source model has provided an unbiased broadband kinematic description of the earthquake source rupture. To examine the trend of the fit over a range of distances, we have computed the synthetic ground motions of the Northridge earthquake at 150 strong

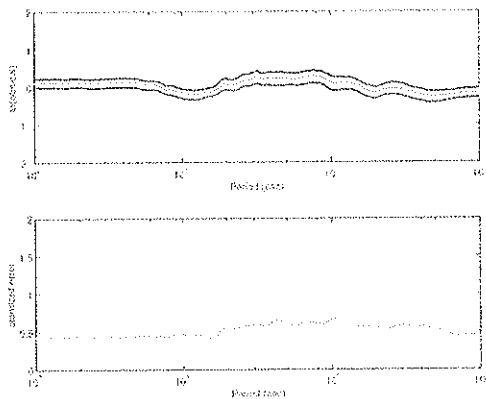


Figure 1. Misfit between the observed and synthetic seismograms for the Northridge earthquake. The upper panel shows the biases (red) and its 90% confidence limits (black) for the horizontal components. The lower panel shows the standard errors.

motion stations. Figure 2 shows the result in comparison with the observed and regression prediction (Abrahamson and Silva, 1997) for PGA and SA at 3 second. The synthetic simulations clearly predict the trends of attenuation of the observed ground motion parameters over distance. The values plotted at the upper right corner of the figures are the standard errors of the prediction from the composite source model and from Abrahamson and Silva's regression respectively. At long period, our synthetic procedure outperformed the regression prediction in terms of both standard errors and distance attenuation rate. Scatter in the data is caused mainly by local site and basin responses.

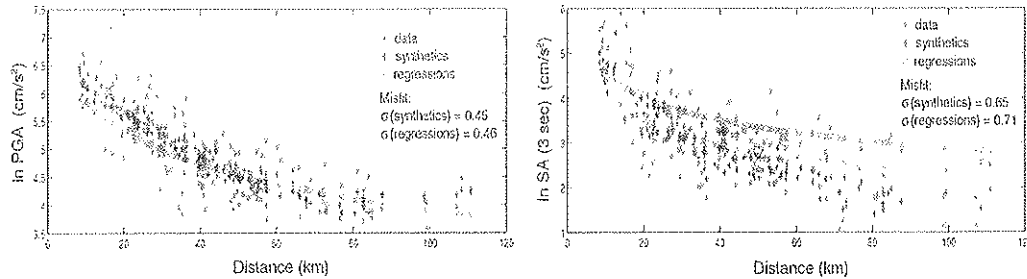


Figure 2. Comparison between observed and predicted peak ground motion parameters for the 1994 Northridge earthquake. The left panel is for the peak ground acceleration and the right panel is for the spectra acceleration with 5% damping at 3 second period.

We have calculated the same misfits as that of Figure 1 but for the Imperial Valley, Loma Prieta, Landers, Kobe, and Kocaeli earthquakes, respectively. In general, we find the simulations are unbiased and the standard errors for all the events are about 0.5 in average (natural log units) across the validation period range. Given those earthquake magnitudes, the results also demonstrate that our ground motion simulation procedure is unbiased for the magnitude range from 6.5 to 7.3.

With the confidence provided by the above validations, we have computed scenario ground motion simulations for the magnitude range from 6.5 to 8.5 at distances from 0 to 200 km. From those simulations, we found the effect of shallow and deep asperities is small. We found large scatter in the synthetic distance attenuation caused by rupture directivity effects. This scatter due to directivity increases as period increases. One interesting observation in the distance attenuation is the effect of the critical Moho reflection. For peak ground acceleration, we found the effect is negligible. At 1 second period, it creates a shoulder in the ground motion attenuation at distance between 60-100 km. At 3 second period, the shoulder moves to 100-140 km. At 10 second period, it moves to 100-200 km. Our interpretation is that the Moho reflection affects the attenuation around 1 second period. For 10 second period, surface waves start to dominate over body waves. For 3 second period, it is a mixed effect of Moho reflection and surface wave generation.

The study of local and regional seismic wave propagation for the Great Basin area started right after the Wells, Nevada earthquake. This earthquake of magnitude 6.0 struck northeastern Nevada on February 21, 2008. It was the largest earthquake to occur in Nevada in the last 30 years. The main shock was followed by thousands of aftershocks (Figure 3). During the time of the main shock and aftershock sequence, the earthscope USArray network was operating in Nevada. As a result, this earthquake sequence was very well recorded and the seismic data from these events provide the best opportunity to study wave propagation in the Great Basin area.

We have collected all the seismic records from this earthquake sequence with magnitude above 4.0 and within an epicentral distance of 300 km from the IRIS data center. We have also carefully picked the S-wave arrival time at each station. All data were corrected for

the instrument responses and then bandpass filtered to calculate the velocity envelopes at different frequencies ranging from 1.5 to 15 Hz.

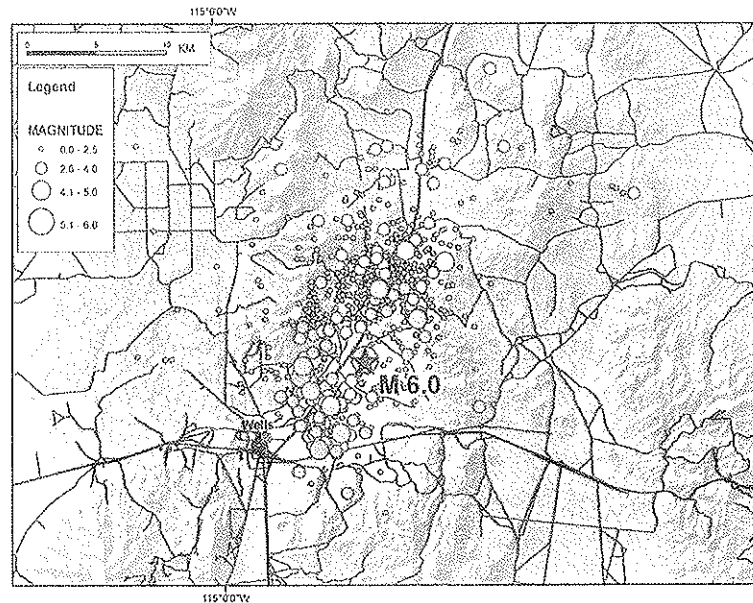


Figure 3. Map view of the Feb. 2008 Well's Earthquake sequence, Nevada.

There are many ongoing studies on the low frequency wave propagation in the Reno and Salt Lake basins in the Great Basin regions (i.e., Liu et al., 2010, Roten, et al., 2010). In this Wells earthquake data analysis, we focus our effort on high frequency waveform modeling. A key part in waveform modeling at high frequency is seismic scattering. Assuming that upon an incident wave energy flux the angular distribution of the scattered energy flux at a scatterer is axially symmetric and non-isotropic, this scattering process can be characterized by a scattering pattern function  $\zeta(\psi)$  (figure 4a) given a scattering angle  $\psi$  from the direction of the incident waves. For an isotropic scattering process, this function equals to  $1/4\pi$ . Figure 4b shows the directional dependent scattering pattern functions for back-scattering (black), isotropic-scattering (purple) and weak/strong forward-scattering (green/red) processes, respectively, on the scattering plane lying along the rays of incidence and scattering.

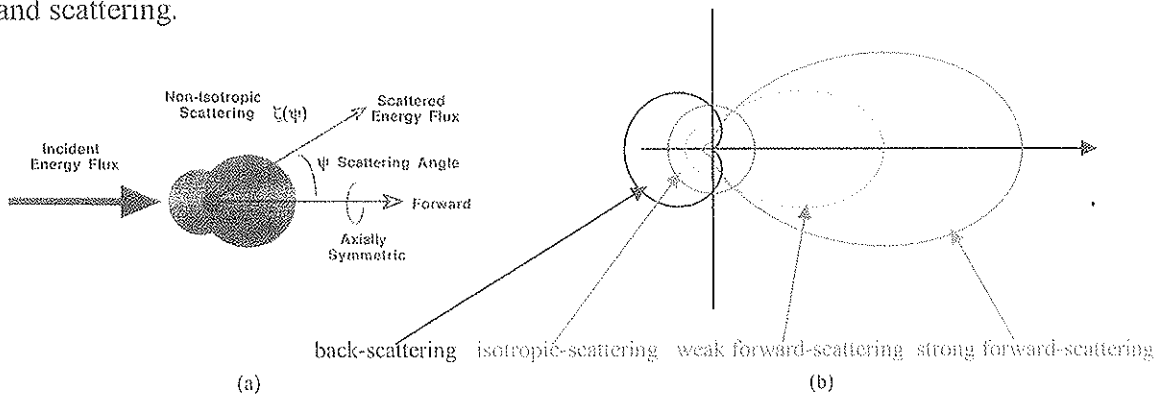


Figure 4. (a) A schematic plot of the angular distribution of a scattering pattern  $\zeta(\psi)$  as a function of the scattering angle  $\psi$  at a scatterer upon incident energy flux (after Sato, 1995). (b) Scattering pattern functions for back-scattering, isotropic-scattering and weak/strong forward-scattering processes, respectively.

In order to study scattering process, we have developed a numerical technique to simulate non-isotropic scattering waves based on the 3-D non-isotropic scattering theory proposed by Sato (1995). We have improved the numerical instability of the hyper-geometrical function calculation in the solutions of the non-isotropic scattering equations. Our numerical tests indicate that different scattering processes result in significant different scattered energy distribution in space. First, we developed a series of scattering patterns (Figure 5, upper right corner) ranging from back-scattering (black color) to strong forward-scattering (Blue color). Base on each scattering pattern we then calculate synthetic velocity envelopes and determined the scattering and intrinsic attenuation coefficients through inversion of the observations.

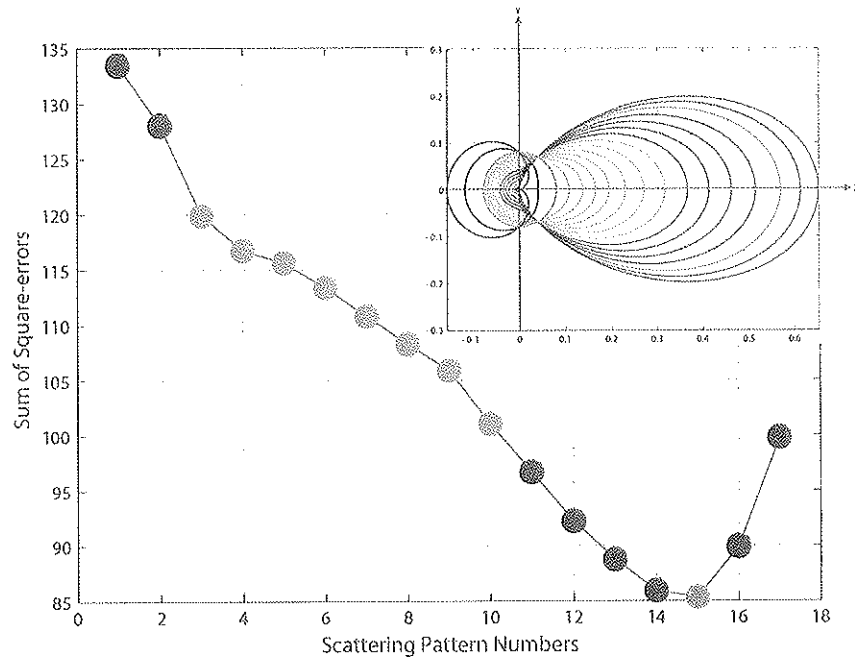


Figure 5. Sum of the square-errors of between synthetic and observed envelope functions versus the scattering pattern models ranging from back-scattering to strong forward scattering.

Figure 5 shows the sum of the square-errors between observation and synthetic envelopes as a function of the scattering pattern. The sum of the square-errors for different scattering pattern is plotted in the same color as the corresponding scattering pattern functions given in the upper right corner of the figure. As shown on figure 5, the two back-scattering models (black color) exhibit the worst fitting to the data. As we gradually decrease the amount of back-scattering and increase the amount of forward scattering, the overall scattering patterns change from back-scattering to isotropic scattering, and then to more and more forward scattering dominated processes. From Figure 5 we can see that the sum of square-errors for isotropic scattering model (pink color) improves over that of the back-scattering models (black color), but the more forward scattering dominated models provide much better fits between observation and synthetics in comparison to the isotropic scattering and back-scattering models. Among the forward scattering models, we can see that for those weak forward-scattering models (green color) their sum of square-errors decreases as the amount of forward scattering increases gradually. The forward scattering model showing in red provided the best fit among all other testing models. After that, the

increasing of forward scattering does not improve the fitting between synthetics and observation. The result suggests that the traditional back-scattering theory (i.e., Aki and Chouet, 1975) does not explain the observations. Instead a forward non-isotropic scattering model provides the best fit to the observed high frequency direct and coda wave energy envelopes.

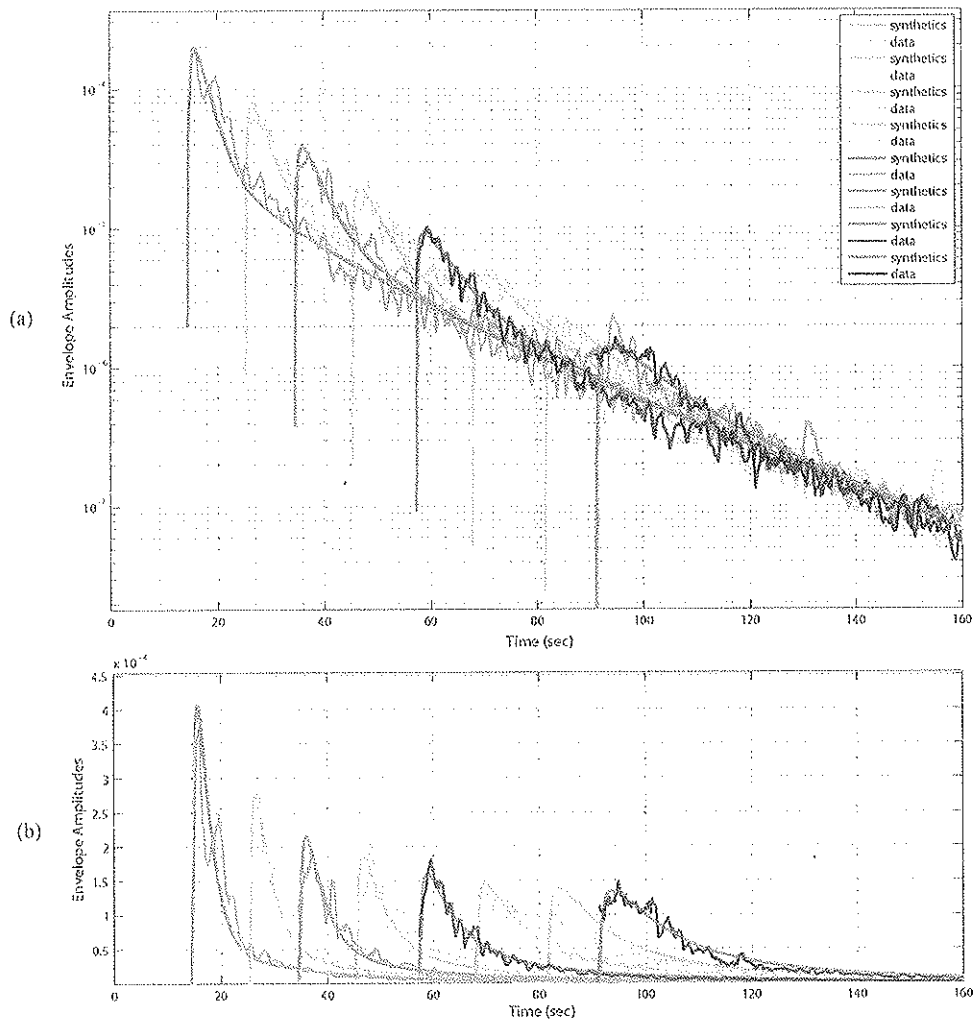


Figure 6. (a) Comparison of the synthetic velocity envelope with the observation in logarithmic scale at selected distances at 12 Hz. (b) The same comparison as in (a) but in linear scale. Both synthetics and observations in (b) are rescaled by  $\exp(0.05 \cdot t_s)$ , where  $t_s$  is the S-wave arrival time for the corresponding stations.

Figure 6 shows the comparison of the synthetic velocity envelopes with observations at 12 Hz at different distances for the best fit scattering model (the forward scattering model shown in red in Figure 5). The observed envelope functions recorded at different distances are indicated by their S-wave arrival times. In order to have a clear view of both direct and coda waves, in Figure 6a, we plotted those envelopes in logarithmic scale. We can see that the synthetic and observation envelopes agree remarkably well for both direct and coda waves at all distances. We also observed a common decay curve in coda independent of station epicentral distances for both synthetics and observations. This

phenomenon was found from observations in 1970s and early 1980s (i.e., Rautian and Khalturin, 1978 and Aki, 1980) and was used for coda renormalization (Aki, 1980) and for estimation of site amplifications (i.e., Phillips and Aki, 1986, Su et al., 1992). In our synthetic test, we found that the common decay observed in seismic coda is also a direct consequence of forward scattering. In Figure 6b we plotted both synthetic envelopes and observations in linear scale to focus at direct waves and early coda. We scaled each envelope function by a factor of  $\exp(0.05*ts)$ , where  $ts$  is its corresponding S-wave arrival time at the station. We can see the synthetic envelopes agree very well with the observations. Interestingly, as distance increases, the pulse widths of those direct S-velocity envelopes also increase. This pulse broadening effect is commonly observed in high frequency wave propagation. Our analysis has demonstrated that the broadening effect is apparently a direct result of forward scattering.

Figure 7 shows the scattering attenuation factor  $Q_{sc}$  (blue) and intrinsic absorption factor  $Q_i$  (red) as a function of frequency for the region determined from the inversion of the observed velocity envelopes using our best fit scattering model. It is clear that the scattering attenuation decreases with increasing frequency, suggesting  $a*k > 1$ , where  $a$  is the length scale of crustal inhomogeneity,  $k=2\pi/\lambda$  is the wave number, and  $\lambda$  is the wavelength. This indicates that the wavelengths of this study are much shorter than the typical length scale of the crustal inhomogeneity in the area. Studies based on multiple lapse-time window data analysis also found similar results in other areas of the world (i.e., Fehler et al., 1992, Mayeda et al., 1992). The intrinsic attenuation  $1/Q_i$  also decreases with frequency, similar to  $1/Q_{sc}$  but gradually flattens towards lower frequency.

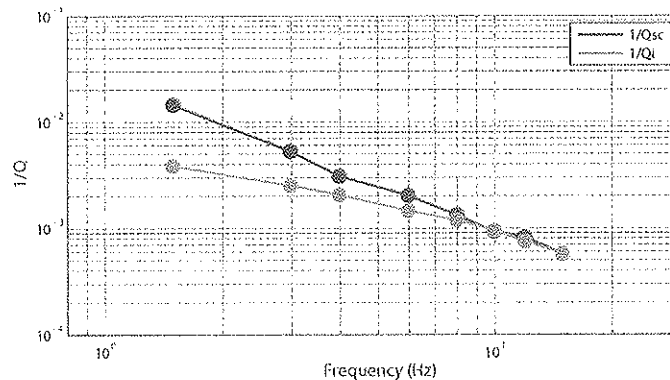


Figure 7. Scattering attenuation factor  $Q_{sc}$  (blue) and intrinsic absorption factor  $Q_i$  (red) versus frequency for the central Nevada region.

Above analysis suggests that seismic coda waves are scattered energy leak out of the forward scattering processes. These results represent a significant step forward in understanding wave propagation in high frequency, especially within the Great Basin.

In conclusion, we have made significant progress during the time span of this project. In the process of our validation and further improvement of our numerical simulation procedure, we have shown that the composite source model has provided an unbiased broadband kinematic description of the earthquake source rupture. At long period, our synthetic procedure outperformed the regression prediction in terms of both standard errors and distance dependent attenuation. From study of source effect on attenuation relation, we

have found that large scatter in the synthetic distance attenuation could be contributed to rupture directivity. This scatter due to directivity increases as period increases. In addition, the critical Moho reflection and surface wave generation have also had significant impact on distance dependent attenuation. In our local and regional seismic wave propagation study in the Great Basin, particularly, in our application to seismic recordings of the 2008 Wells, Nevada earthquake sequence, we found that traditional back-scattering theory does not explain the observations. Forward non-isotropic scattering model provides the best fit to the observed high frequency envelopes. These results are very important to further development of ground motion attenuation relations in the Great Basin based on a combined empirical and synthetic dataset. The results from this project will directly contribute to the prediction of strong-ground motion and seismic hazard assessment in the Great Basin.

## References

Abrahamson, N. A. and W. J. Silva (1997). Empirical response spectral attenuation relations for shallow crustal earthquakes. *Seism. Res. Lett.* **68**, 94-127.

Aki, K., and Chouet, B. (1975), Origin of Coda Waves: Source, Attenuation and Scattering Effects, *J. Geophys. Res.* **80**, 3322-3342.

Aki, K. (1980), Attenuation of Shear-waves in the Lithosphere for Frequencies from 0.05 to 25 Hz, *Phys. Earth Planet. Inter.* **21**, 50-60.

Fehler, M., Hoshihara, M., Sato, H., and Obara, K. (1992), Separation of Scattering and Intrinsic Attenuation for the Kanto-Tokai Region, Japan, Using Measurements of S-Wave Energy Versus Hypocentral Distance, *Geophys. J. Int.* **108**, 787-800.

Liu, Q., R.J. Archuleta, R.B. Smith (2010). Ground Motion from Dynamic Ruptures on the Wasatch Fault Embedded in a 3-D Velocity Structure, *Seism. Res. Lett.* **81**, p320.

Mayeda, K., S. Koyanagi, M. Hoshihara, K. Aki and Y. Zeng (1992). A comparative study of scattering, intrinsic, and coda  $Q^{-1}$  for Hawaii, Long Valley and Central California between 1.5 and 15 Hz, *J. Geophys. Res.* **97**, 6643-6659.

Phillips, W. S. and K. Aki (1986). Site amplification of coda waves from local earthquakes in central California, *Bull. Seismol. Soc. Am.* **76**, 627-648.

Rautian, T. G. and V. I. Khalturin (1978). The use of the coda for determination of the earthquake source spectrum, *Bull. Seismol. Soc. Am.* **68**, 923-948.

Roten, D., K.B. Olsen, J.C. Pechmann, V.M. Cruz-Atienza, H. Magistrale (2010). Ground Motion Predictions from 0-10 Hz for M7 Earthquakes on the Salt Lake City Segment of the Wasatch Fault, Utah, *Seism. Res. Lett.* **81**, p320.

Sato, H. (1995). Formulation of the multiple non-isotropic scattering process in 3-D space on the basis of energy transport theory, *Geophys. J. Int.* **121**, 523-531.

Su, F., K. Aki, T. Teng, Y. Zeng, S. Koyanagi and K. Mayeda (1992). The Relation Between Site Amplification Factor and Surficial Geology in Central California, *Bull. Seism. Soc. Am.*, **82**, 2, 580-602.

Zeng, Y., J. G. Anderson and G. Yu (1994). A composite source model for computing realistic synthetic strong ground motions, *J. Res. Lett.*, **21**, 725-728.